ISTITUTO NAZIONALE DI FISICA NUCLEARE

Sezione di Milano

INFN/TC–99/23
21 Ottobre 1999

EXPERIMENTAL RESULTS OF FAST X–RAY IMAGING WITH A SILICON PIXEL DETECTOR FOR THE FEASIBILITY OF AN AUTOMATIC TUMOR X–RAY SURVEY AND TRACKING SYSTEM

P.W. Cattaneo[1], P. Musico[2], B. Osculati[2], N. Redaelli[3], M. Sciutto[2], S. Squarcia[2]

[1)] INFN – Sezione di Pavia Via Bassi, 6 – 27100 Pavia, Italy
[2)] INFN – Sezione di Genova, Dipartimento di Fisica, Via Dodecaneso 33 –16146 Genova, Italy
[3)] INFN – Sezione di Milano, Via G. Celoria 16 – 20133 Milano, Italy

Abstract

The results of a test of OMEGA3/LHC1 hybrid silicon pixel detectors as fast X–ray digital imaging apparatus during oncological hadron therapy are reported; the tested detectors show a good sensitivity for low–contrast phantoms. Design modifications for a detector optimization in oncological applications are discussed.

PACS.: 07.85

*Published by **SIS–Pubblicazioni***
Laboratori Nazionali di Frascati

1 INTRODUCTION

This paper describes an experimental test of silicon pixel detectors as a fast X–ray digital imaging apparatus for automatic tumor positioning during oncological hadron therapy.

This feasibility test has been performed in the framework of the ATER experiment financed by I.N.F.N[1)], devoted to the development of the apparatus for the TERA hadron therapy project[2)], and it has been realized using the Genova pixel test set–up of the ATLAS experiment[3)]. In the following, we briefly recall the motivations of this feasibility test, a detailed description can be found elsewhere .

In each therapy treatment session with hadron beams, the tumor irradiation lasts some tens of seconds. The geometrical precision of the energy deposition is one of the main features of the hadron therapy method: the definition of the zone where the beam protons release most of their energy can be as precise as 1 mm. The tumor position must then be known with a similar precision during the whole therapy session.

In this time interval, different factors could affect the correct positioning of the tumor, and induce misalignment of the hadron beam: physiological movements, as breathing, and unpredictable sudden movements of the patient.

In the framework of the ATER collaboration, we proposed a test to evaluate the feasibility of a fast X–ray digital imaging of the tumor during the hadron therapy session. An on–line imaging could allow fast feedback on the beam controlling system, to follow the tumor in its movements.

An estimate of the rapidity of the possible movements of the patient gives a lower limit to the frequency of the control process needed to guarantee the precision of 1 mm in the tumor positioning. The complete control process, consisting of the image acquisition, of the software image filtering and comparison of the tumor position with the reference position, and of the consequent feedback on the beam, must be completed in a total time of 100 ms[4)]. It must be considered that diagnostic accurate TAC or NMR images of the tumor will be available, so that the image recognition during the control process will be easy. That is, image recognition is limited to pre–defined well–known shape.

A complete study of the potentiality of this project involves the biological characterization of different tumors, in order to investigate their visibility with an X–ray digital imaging apparatus.

X–ray imaging in biomedical applications has already been performed by means of Charged Coupled Devices (CCD). In our case we need signal processing faster than CCD. Although silicon is far from being of high intrinsic efficiency in X–ray detection, pixel detectors have been already successfully employed in X–ray imaging on scintillating crystals and scintillating fibers as described in[5)].

In order to satisfy the requested timing of the complete control process we chose to employ pixel detectors.

We restrict our study to evaluate the performances of silicon pixel detectors as a fast X–ray digital imaging apparatus. Between a diagnostic X–ray tube and the pixel detectors

we interposed specimens of different materials and shapes, in order to measure the apparatus contrast capability.

Some peculiar characteristics of the pixel detectors indicate these detectors as a most promising choice to meet the specifications of our experiment. Pixel detectors are intrinsically unambiguous bidimensional detectors. This geometrical property provides an advantage in the low–efficiency photoelectric detection. Pixel detectors have a fast signal processing; they produce a digital output signal and they have quasi–parallel readout architecture.

All these features considerably reduce the time spent for the signal detection and for the front–end signal processing, leaving a larger time for the on–line image recognition and the beam feedback.

2 EXPERIMENTAL SET–UP

The X–ray source is a diagnostic X–ray tube with a photon energy range 10 to 60 keV. The X–ray beam is collimated to cover the active surface of a pixel detector positioned 30cm downstream. In the space between the X–ray tube and the detector we interposed specimens of various materials and shapes, the distances being similar to the distances in the future medical applications: an X–ray beam impinging on one side of a patient body and an array of pixel detectors positioned on the other side.

The X–ray tube, the pixel detector and the first card of the readout electronics are located inside a shielded box, for radiation safety reason. The signal readout, the bias and the control signals cables exit the box and are connected to the VME crate for data acquisition, bias supplies, control signals supplies and pulse generator, as shown in Fig.1.

The data–taking programs are executed on a VME FIC 8234 controller with a Motorola 68040 microprocessor, which dialogs through the VME bus with the peripheral electronics card (master board in the figure). This assures, through a slave board, the connection between the VME system and the pixel front–end electronics, described in the following sections. A pulse generator provides the strobe signal to trigger the data acquisition, and can also be used to calibrate the pixel electronics. After acquisition, the data are transferred to a PC, where they are analyzed.

2.1 The hybrid pixel detector and the OMEGA3/LHC1 chip

The detectors we used are the OMEGA3/LHC1 pixel detectors, developed by the RD19 CERN Collaboration[6)] for high–energy experiments. They performed well in the heavy–ions CERN experiment WA97[7)], and are an evolution from former versions[8)] in the framework of a R&D activity to optimize a vertex pixel detector for the future LHC experiments at CERN.

The OMEGA3/LHC1 detectors are hybrid silicon pixel devices: each high resistivity, 300 μm thick, silicon pixel detector is connected to its VLSI front–end readout cell using the bump bonding technique[9)].

The pixel detector consists of two plates, the first plate being the silicon active crystal and the second plate the electronics chip bonded to the crystal. Our detector is 0.64 cm long and 0.8 cm wide, corresponding to an active surface of 0.5 cm^2.

The pixel structure of the chip is organized in 128 rows and 16 columns, the dimension of each pixel being 50 μm by 500 μm, for a total number of 2048 pixels. A detailed description of the OMEGA3/LHC1 VLSI front–end chip can be found in [10]. Here we only recall its basic features illustrated in Fig. 2.

The elementary VLSI cell consists of a front–end charge preamplifier coupled to the corresponding active pixel, followed by an asynchronous comparator, a delay line and a memory unit (flip–flop, D in the figure).

The asynchronous comparator threshold (Th in the figure) is externally adjustable linearly between 3000 and 15000 electrons, the delay line (D_1, D_2, D_3 in the figure) is locally fine tunable by a 3 bit delay line element (DL_0, DL_1, DL_2 in the figure). From the comparator a fast–or output can also be extracted, which can be used for self–triggering.

During the data acquisition, the signal of the front–end charge preamplifier is compared in each pixel to the comparator threshold. The output level of the comparator is set when the signal is over the threshold. The comparator signal is delayed to allow a coincidence with the strobe signal coming from the trigger pulse produced by the data acquisition system. The delay line allows a fine tuning of the coincidence delay. If there is a coincidence, a local memory flip–flop is set (in the following this will be called hit pixel), otherwise the event is lost. The strobe signal is common to all pixels.

All the data flip–flop elements of a detector column are connected in series and constitute a shift register to readout the single pixel digital signal. A parallel transfer of the binary map of the 16 column shift registers realizes the readout of one chip.

This operation starts at the end of the strobe signal and requires a number of clock pulses equal to the number of rows to be read (i.e. 128); with a 40 MHz clock the total time required to read the detector is 3.2 ms.

The data transfer from the chip up to the slave card is on a 16 bit bus synchronous with a 40 MHz clock. The transfer from the slave to the master card also uses a 16 bit bus, but with an asynchronous protocol that slows down the process, and the total acquisition time is on the order of a millisecond.

2.2 The controller chip (COOP)

In order to build larger detection surfaces it is foreseen to use several OMEGA3/LHC1 chips organized in groups (ladders) of six consecutive chips mounted side by side on a ceramic substrate, of which the overall dimensions are 4.8 cm by 0.64 cm. Several ladders could then be placed staggered and side–to–side to construct large–area detector surfaces. When pixel detectors are used in a multi–ladder configuration, it is necessary to implement a control system common to several chips. This is achieved by means of the COOP chip described below and developed by the Genova group in the framework of the ATLAS collaboration. A detailed technical description of

the COOP can be found in[11]. This chip has been conceived to handle the control of ladders of OMEGA3/LHC1 chips. A ladder plane of 5 cm by 5 cm could be driven by 8 COOP chips.

The principal COOP functions are:

Produce the strobe signal for all the OMEGA3/LHC1 chips of one ladder with a variable delay in a 250 ns time interval set by the data acquisition program;

Read and write chip parameters independently on a specific ladder;

Produce all the analog levels necessary to set the detector–chip working conditions as, for example, the comparator threshold value. This setting can be adjusted independently on each chip;

Set all the working parameters of the OMEGA3/LHC1 chip;

Allow an automatic readout of the data taken by the detector transferring only the coordinates of the hit pixels.

This last feature of the COOP enables to speed up the data transfer procedure when there is only few hit pixels.

The COOP chip makes it possible to tune all the analog signals that control the chip behavior, like: threshold, delay, fine–delay, comparator bias, preamplifier bias. In our test we exploited the possibility to vary the strobe delay at the single pixel level, timing the apparatus with a pulse–generator test run.

Our test is performed with only one single detector OMEGA3/LHC1 chip connected to the COOP chip.

2.3 The X–ray tube

The used source is an X–ray tube for dental diagnostic, with a W target, whose maximum energy of 60 keV can be reduced by acting on the electron acceleration voltage. The X–ray intensity, which cannot be varied, was roughly measured using a Si photo–diode p–i–n (mod. BPW34)[12]. On the tube opening the measured absorbed dose on silicon was about 7300Gy/h. The distance of our detector from the tube (of the order of 30 cm) reduces this dose by a factor of 900. The maximum time of continuous running of the tube can be varied up to 3s, and we chose this maximum value for our acquisition runs.

3 EXPERIMENTAL RESULTS

Our aim is to verify the imaging capability of our detector as X–ray imaging apparatus. We first operated preliminary tests using radioactive ß ^{90}Sr sources, and interposing selective screens of different material and thickness between the source and the detector. As explained, a trigger drives the data acquisition of our detector. In order to deal with the Poisson distribution of the radioactive decays, we chose not to implement an external trigger. We simply tuned the duration of the strobe to the source intensity, to have a reasonable probability to trigger events, reducing in the same time the pile–up probability.

The binary map of each elementary acquisition (elementary image) was readout, and a complex image is the superimposition of many elementary images. The bottleneck of the

acquisition was the asynchronous part of the readout, bringing to the order of the millisecond the time needed for an elementary image (see section 2.1).

In the following, in our image analysis, we will characterize the imaging capability of our apparatus by the Signal–to–Contrast (SC) ratio, defined as

$$SC = (B - S)/B, \quad (1)$$

where S is the average number of photon–counts per pixel in the signal region and B is the average number of photon–counts per pixel in the background region.

3.1 Imaging of low–Z phantoms

In order to run the data–taking of one complex image with the X–ray tube, we had to take into account the time needed for the acquisition of an elementary image, the X–ray initial transient behavior and the maximum time of continuous running, and therefore we preset the acquisition of 800 elementary images, starting after the transient phase.

Two parameters are the most critical to set during the data acquisition: the strobe duration, to be tuned, as explained, to the X–ray source and the comparator threshold. To define the best running condition for X–ray imaging, we took images with different strobe duration, keeping all other parameters unchanged. By a simple comparison of the mean number of photon counts per pixel in the complex images, we were able to optimize the efficiency, meanwhile keeping the pile–up under control. Our choice for the strobe duration was 100 μs.

The comparator threshold was set to 10000 e^-. This threshold value is rather high, and it is motivated by the prolonged strobe duration, which causes an increase of the noise[1].

The threshold is common to all the pixels in one chip. We took images irradiating the chip uniformly, thus the differences in the single–pixel counts should be contained in the Poisson errors. On the contrary, we observed more relevant fluctuations (see Fig.3): in fact even small single–pixel threshold non–uniformities produce relevant consequences, since the silicon detection efficiency is higher at lower energies[13)], and we are dealing with a continuous energy spectrum.

We cannot evaluate rigorously our detector efficiency, since we have only an integral measurement of the dose on silicon and we do not know the actual energy spectrum of our X–ray source. An estimate can be attempted under some assumptions. The X–ray source intensity is estimated[14)] assuming a mean energy value of 50 keV, and the corresponding photon absorption coefficient in silicon of 0.4 cm^2/g. We can then evaluate the efficiency as the mean number of photon counts per pixel in a complex image normalized by the time–integrated photon flux per pixel.

[1] In high–energy applications, the typical strobe duration is set to 50 ns and the applied threshold value is of the order of 4500 e^-

Due to the uncertainties of our assumptions, we take our efficiency estimation, of the order of 0.7 %, only as an indicative value. The expected efficiency for a 300 μm thick silicon detector is of the order of 1 % [13].

As first selective screen, we inserted between the X–ray source and the detector a brass grid (pitch 1.5 mm and thickness 500 μm). In Fig.4, the visibility of the rough image, without any elaboration, can be appreciated.

We then took images interposing low–Z selective screens. The first screen was a 3 mm thick Plexiglas layer (Polymethyl Methacrylate, $Z_{mean} = 3.6$), which we positioned to cover a part of the detector. The threshold fluctuations prevented from a first–sight appreciation of the contrast. To overcome the problem and roughly equalize the pixel response, we subtracted the matrix of the single–pixel photon counts of our image from the matrix of the single–pixel photon counts of a reference image, taken without any interposed obstacle. In this threshold–equalized image we measured the Signal–to–Contrast ratio to be $SC = 0.14 \pm 0.06$. The expected value, obtained under the assumption of a mean X–ray energy value of 50 keV, is $SC_{th} = 0.10$.

We proceeded to analyze the imaging capability with a series of PVC (PolyVinyl Methacrylate, $Z_{mean} = 5.3$) low–contrast phantoms: the phantoms were of different thickness, ranging from 5 mm to 1 mm.

We produced threshold–equalized images, using the same procedure as with the Plexiglas screen. In Fig.5 the SC values are reported as a function of the phantom thickness. The linear correlation between the phantom thickness and the visibility can be clearly appreciated.

In medical applications the tumor must be recognized inside the human body, the density of which is usually represented by water. We therefore performed a visibility test of low–contrast specimens immersed into water. We positioned our PVC specimens in the center of a cylindrical vessel with diameter of 8 cm, filled with water; the vessel was made of a thin PET (PolyEthilen Therphthalate) layer. The water environment has a higher photon absorption probability with respect to the air environment; a complex image was then obtained by superimposing 8000 elementary images, 10 times the number of the elementary images superimposed in the analysis discussed above, to reduce the fluctuations in the single–pixel counts.

The threshold equalization was performed with the above described method, the reference image was taken with the vessel filled with water without any immersed specimen.

The complex image of a 3 mm side PVC cubic specimen, supported by a thin iron stick glued on a side and immersed into water is reported in Fig.6: the small PVC cube is well visible in the water background, with the lateral iron support on the left of the PVC specimen.

In this last case the dose delivered to the specimen is quite hight but it should be kept in mind that we were obliged to have a high irradiation because of the threshold non uniformity problem. In a VLSI chip specifically thought for X rays imaging the uniformity

of the threshold values of each pixel should be carefully considered: a detector with threshold control on the single pixel would allow an equivalent contrast with considerably reduced dose. Calculations of the dose delivered with X rays to the patient during a hadron therapy session, using such an optimized detector , show that it is of the order of 0.1 % of the dose delivered by the hadron therapy beam to the patient.

4 CONCLUSIONS AND PERSPECTIVE

Our feasibility test of pixel detectors as fast X–ray imaging detector gives a positive result. The employed detector shows a good sensitivity for low–contrast phantoms, and looks promising for the proposed survey application. The employed detector, the Omega3/LHC1 pixel detector, being conceived for high–energy physics applications, would need some targeted design modifications to be optimized for our applications; in the following we list the most significant ones:

The detector should have a squared geometry, and the pixel dimension should be of the order of 200–300 μm;

The silicon sensor has a poor efficiency as X–ray detector; Ga–As sensors would produce a relevant gain in efficiency, and a consequent reduction in the X–ray dose to the patient;

The threshold value is now common to the whole chip, and it produces large fluctuations in the single–pixel answers; a gain in uniformity would be obtained by a threshold control on the single pixel;

A continuous front–end processing should be more performant than the current trigger–driven acquisition;

The data acquisition has a bottleneck in the asynchronous transfer to the VME system, that brings to the order of a millisecond the time needed for the acquisition of an elementary image; a counter on the front–end chip should store the histogram of the superposition of many elementary images, and the time for transferring would be spent only once, for the complex image.

Different groups are carrying on a promising R&D activity on the design of pixel detectors optimized for medical applications [15)].

Encouraged by our present result, we conclude that pixel detectors optimized with respect to the points listed above will likely meet all the requirements as fast X–ray digital imaging apparatus for automatic tumor positioning during oncological hadron therapy.

5 ACKNOWLEDGEMENTS

We are grateful to the Genova ATLAS group for technical support. We want also to thank many colleagues who very kindly lent us electronic instrumentation to set up our laboratory, and particularly the Genova INFN Gruppo II and E. Bellotti from Milano. Special thanks to P. Ottonello who lent us the X–ray tube. One of the authors (N. Redaelli) wishes to thank C. Da Via for suggestions and encouragement at the beginning of this work.

6 REFERENCES

(1) Istituto Nazionale di Fisica Nucleare – Gruppo V, Piano Triennale 1999–2001 di Ricerche e Sviluppo in Adroterapia, ATER2, (Milano, 25 Giugno 1998).

(2) TERA Collaboration, “The TERA project and the centre for oncological hadron therapy”, INFN–LNF–Divisione Ricerca, Ufficio Pubblicazioni, Frascati. Editors U. Amaldi and M. Silari (1994).

(3) ATLAS Technical Proposal, (CERN/LHCC/94–43 LHCC/P2, 1994).

(4) G. Baroni et al., “New methods for patient alignment”, Excerpta Medica, International Congress Series, p. 278, (1997).

(5) C. Da Via et al.:RD19 Collaboration: “Experimental results using a hybrid silicon pixel detector for scintillating fibre readout and X–ray imaging”, IEEE Transaction on Nuclear Science, **42**, p. 409, (1995).

(6) F. Anghinolfi et al. – RD19 Collaboration, “Status report RD19 development of hybrid and monolithic silicon micropattern detectors”, CERN/DRDC 92–5 (1991).

(7) D. Di Bari et al., “Performance of 0.5 10^6 sensitive elements pixel telescope in the WA97 heavy–ion experiment at CERN”, Nucl. Instrum. Methods A, **395**, p. 391, (1997).

(8) F. Anghinolfi et al. – RD19 Collaboration, “A 1006 element hybrid silicon pixel detector with strobed binary output”, IEEE Transaction on Nuclear Science, **39**, p. 654, (1992).

(9) D.J. Pedder, “Flip–chip solder bonding for advanced device structure”, Plessey Research Review, p. 69 (1989).

(10) E.H.M. Heijne et al., “LHC1: A semiconductor pixel detector readout chip with internal, tunable delay providing a binary pattern of selected events”, Nucl. Instrum. Methods A, **383**, p. 55, (1996).

(11) G. Darbo and P. Musico, “The Controller for the Omega Pixel (COOP) chip and its readout system”, Draft in preparation, INFN Genova.

(12) P.W. Cattaneo,” Calibration procedure for irradiation test on silicon device”, IEEE Transaction on Nuclear Science, **38**, p. 1, (1991).

(13) S.R. Amendolia et al., “A project for digital mammography based on a GaAs pixel detector and on a self–triggering single photon counting acquisition system”, Physica Medica, **13**, p. 157, (1997).

(14) R.M. Barnett et al., “Particle Data Group”, Phys. Rev. D, **54**, p. 194, (1996).

(15) C. Da Via et al., “Gallium arsenide pixel detectors for medical imaging”, Nucl. Instrum. Methods A, **395**, p. 148, (1997).

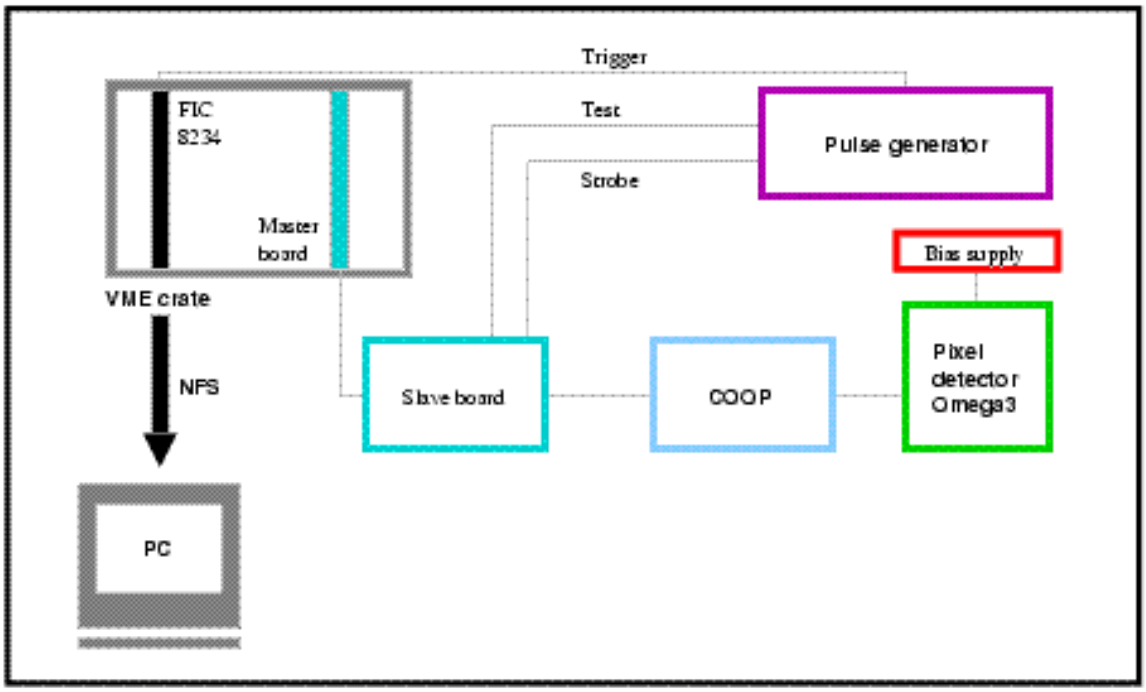

Fig. 1 – layout of the acquisition set–up.

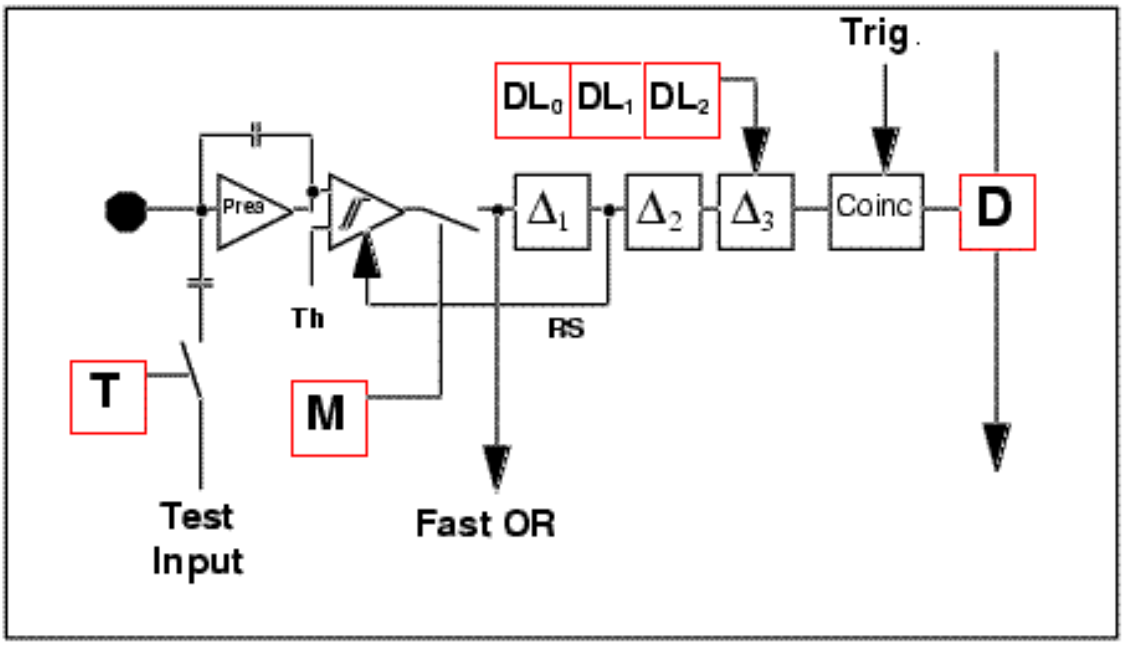

Fig. 2 – The front–end circuit of the OMEGA3/LHC1 cell.

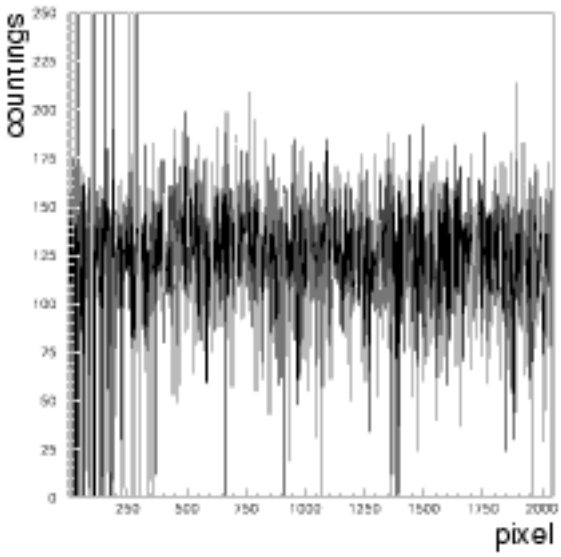

Fig. 3 – Single pixel counts in a uniformly irradiated chip: the large fluctuations arise from the common threshold value.

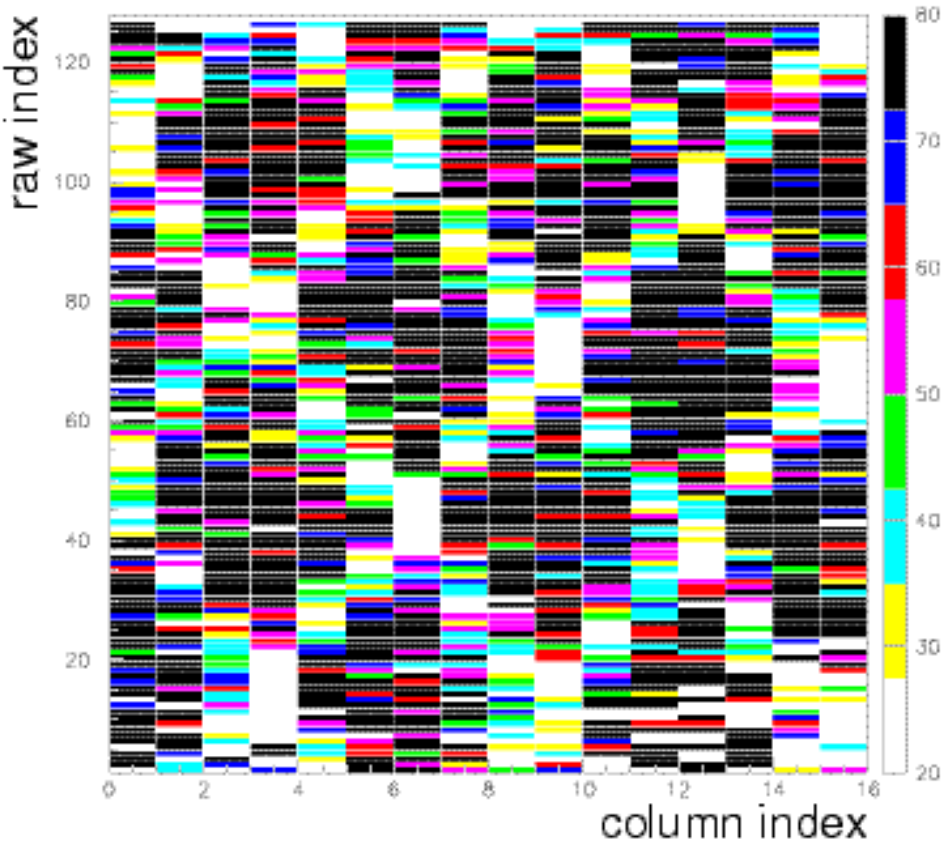

Fig. 4 – X–ray image of a brass grid (pitch 1.5 mm and thickness 500 μm). The dimensions of the single pixels are 500 μm in the column coordinate and 50 μm in the raw coordinate.

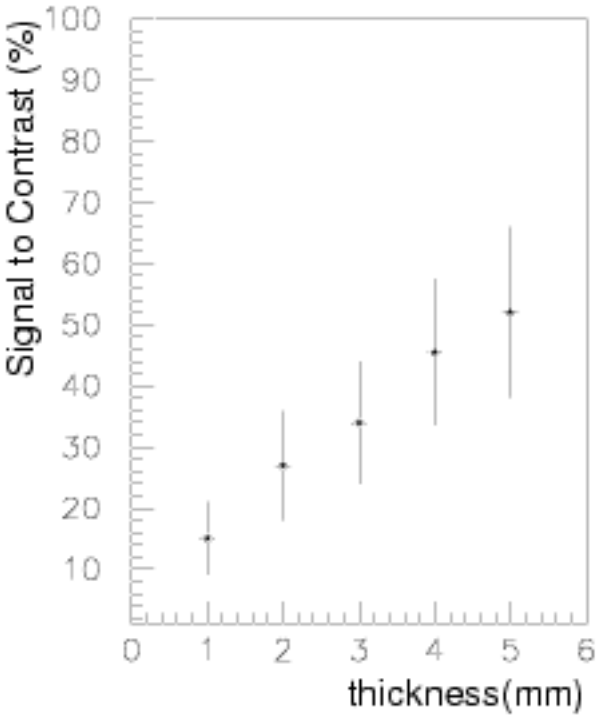

Fig. 5 – Signal to Contrast ratio for PVC specimens of different thickness.

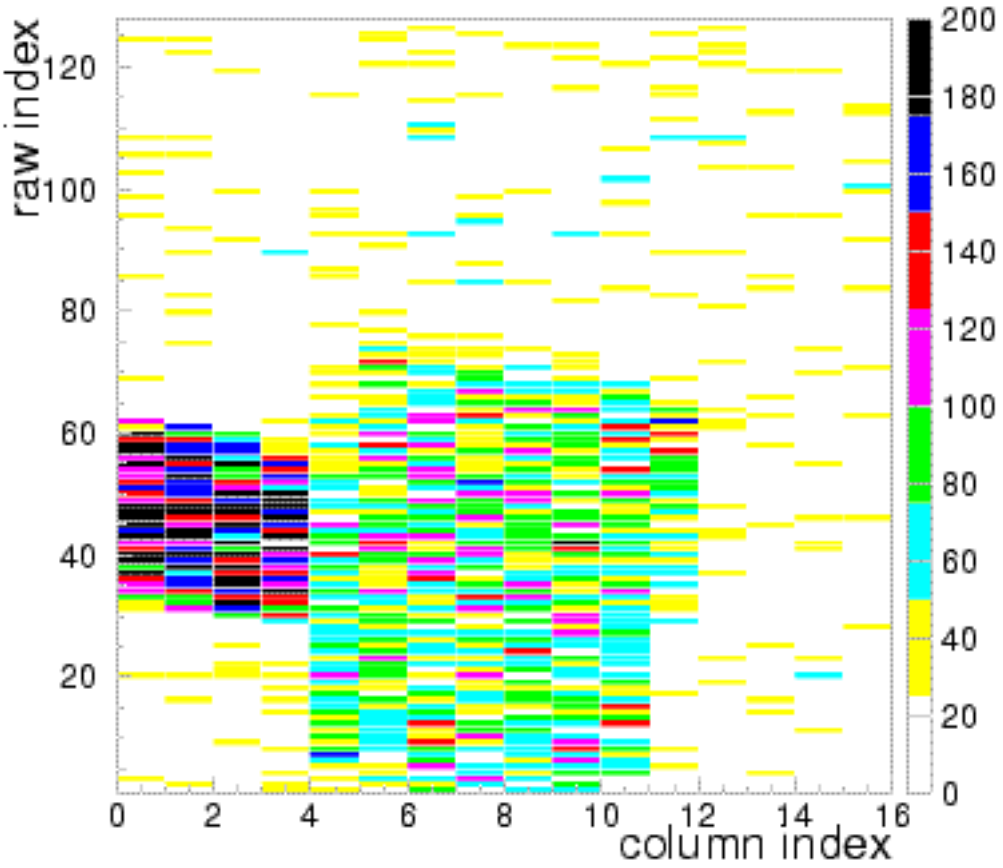

Fig. 6 – X–ray image of a cubic PVC specimen immersed into water. On the left side of the PVC specimen, the thin iron support is visible. The dimensions of the single pixels are 500 μm in the column coordinate and 50 μm in the raw coordinate.